ORIGINAL PAPER

Microwave-Triggered Chemiluminescence with Planar Geometrical Aluminum Substrates: Theory, Simulation and Experiment

Michael J. R. Previte · Chris D. Geddes

Abstract Previously we combined common practices in protein detection with chemiluminescence, microwave technology, and metal-enhanced chemiluminescence to demonstrate that we can use low power microwaves to substantially increase enzymatic chemiluminescent reaction rates on particulate silvered substrates. We now describe the applicability of *continuous aluminum metal substrates* to potentially further enhance or "trigger" enzymatic chemiluminescence reactions. Furthermore, our results suggest that the extent of chemiluminescence enhancement for surface and solution based enzyme reactions critically depends on the surface geometry of the aluminum film.

In addition, we also use FDTD simulations to model the interactions of the incident microwave radiation with the aluminum geometries used. We demonstrate that the extent of microwave field enhancement for solution and surface based chemiluminescent reactions can be ascribed to "lightning rod" effects that give rise to different electric field distributions for microwaves incident on planar aluminum geometries. With these results, we believe that we can *spatially* and *temporally* control the extent of *triggered* chemiluminescence with low power microwave (Mw) pulses and maximize localized microwave triggered metal-enhanced chemiluminescence (MT-MEC) with optimized planar aluminum geometries. Thus we can potentially further improve the sensitivity of immunoassays with significantly enhanced signal-to-noise ratios.

Acronyms and symbols

BSA	Bovine Serum Albumin
FDTD	Finite-Difference Time Domain
HRP	Horseradish peroxidase
MAMEF	Microwave-Accelerated Metal-Enhanced Fluorescence
MEF	Metal-Enhanced Fluorescence
MT-MEC	Microwave-Triggered Metal-Enhanced Chemiluminescence
Mw	Low-Power Microwave heating

M. J. R. Previte · C. D. Geddes (✉)
Institute of Fluorescence, Laboratory for Advanced Fluorescence Spectroscopy & Laboratory for Advanced Medical Plasmonics, Medical Biotechnology Center, University of Maryland Biotechnology Institute,
725 West Lombard St., Baltimore, MD 21201, USA
e-mail: geddes@umbi.umd.edu

C. D. Geddes
Center for Fluorescence Spectroscopy, Medical Biotechnology Center, University of Maryland School of Medicine,
725 West Lombard St, Baltimore, MD 21201, USA

Introduction

Previously, we described a new platform technology, microwave triggered metal-enhanced chemiluminescence (MT-MEC) [1, 2]. With this technology, we alluded to its potential to improve the sensitivity of bioanalytical applications, such as immunoassays, antioxidant assays, microbiology, protein blotting, nucleic acid analysis, cellular studies, cancer detection and disease screening [1–3]. While chemiluminescent reactions have become the method of choice for protein detection assays [4], immunoassays [3–10], and small molecule

detection in more than 20% of clinical laboratories in the United States [8], the sensitivity of these reactions still remains limited by the fundamental detection limits, i.e., poor signal-to-noise ratios at low analyte concentrations. Thus, the sensitivity and specificity of these reactions require further improvements to facilitate early diagnosis of disease.

With the application of microwave pulses, we have demonstrated that we can 'trigger' HRP enzyme catalyzed chemiluminescent reactions and create large 'on demand' photon bursts (i.e., flux) from the reaction [1, 2]. In addition, in the presence of silver island films, the chemiluminescence emission is not only enhanced from the plasmon effects of chemiluminescence coupled to silver surfaces [1, 2, 11, 12], but also the reaction is further accelerated and 'triggered' by the localized heating of the metal colloids [13, 14]. Subsequently, we can provide marked improvements in the fundamental detection limits of chemiluminescent reactions catalyzed enzymatically with horseradish peroxidase (HRP) [2].

The use of microwave radiation has greatly increased over the past two decades in radar and communication systems [15], for accelerating reactions in synthetic organic chemistry applications [16–18], in drug delivery [19], assays [20–24] and in biochemistry [25–27]. The concept of creating localized and amplified microwave fields is actively researched and explored in detail for applications in microwave circuitry and antenna design [28]. Considering our recent work on microwave-based, triggered metal-enhanced chemiluminescence (MT-MEC), combined with the knowledge that microwaves can localize around geometric metallic shapes, most notably aluminum, we now show that we can use thin film aluminum square geometries to localize microwave fields from low power 2.45 GHz microwave pulses. Subsequently, we can use these localized fields to 'trigger' or amplify localized photon flux from both surface and solution based enzyme-catalyzed chemiluminescent reactions.

In addition, we have used FDTD simulations to model the interactions of the incident microwave radiation with the aluminum geometries used in these experiments. We can now demonstrate that the extent of microwave field enhancement for solution and surface based chemiluminescent reactions can be due to "lightning rod" effects that give rise to different electric field distributions [29] on planar aluminum geometries. Consistent with these findings, we show experimentally that we can *spatially* and *temporally* control the extent of *triggered* chemiluminescence from solution and surface based reactions with low power microwave (Mw) pulses and maximize localized microwave field enhancements with optimized planar aluminum geometries.

Due to increased reaction rates for these triggered chemiluminescent reactions on aluminum substrates, the 'on-demand' nature of light emission provides substantial improvements in signal-to-noise ratios and a spatially local-

ized amplified photon flux for discrete time intervals. We believe that these results demonstrate a potentially, promising new, inexpensive microwave technology that may prove beneficial across many scientific disciplines, most notably, organic synthesis [14, 15, 17, 18, 30], in enhancing rates of enzymatic reactions [1, 2, 12, 20, 25, 26, 31], medicine [19, 32–34], bioanalysis [1, 2, 16, 26], and clinical sensing [20, 35].

Experimental

Materials

Bovine-biotinamidocaproyl-labeled Albumin (biotinlyated BSA), HRP-labeled avidin, 99.999% aluminum evaporation slugs, silicon monoxide pieces, and premium quality APS-coated glass slides (75×25 mm) were obtained from Sigma-Aldrich. CoverWell imaging chamber gaskets with adhesive (5 mm diameter, 2 mm deep) were obtained from Molecular Probes (Eugene, OR). Steptavidin-HRP pre-diluted solution (Catalog # 20774) was obtained from Chemicon® International Inc. Chemiluminescence reagents for these experiments were purchased from Amersham Biosciences (ECL Plus™ Western blotting detection kit, RPN2132).

Chemiluminescence reagents

The ECL™ Western Blotting Detection Kit contained two reagents that yield a bright chemiluminescent emission at 430 nm upon mixing. Solution A contained the substrate solution (peroxide formulation) and solution B contained the solution of the luminescent compound, acridan in dioxane and ethanol. HRP and hydrogen peroxide solution (solution A) catalyze the oxidation of the acridan substrate (solution B). As a result, acridinium ester intermediates are formed and further react with peroxide to generate light emission with a maximum wavelength centered around 430 nm.

FDTD software and computation

FDTD software was purchased from Lumerical Solutions, Inc., to solve Maxwell's equations for structures that have complex geometries and/or widely varying electromagnetic material properties for a wide variety microwave field sources. With this software package, we can record time domain information at any spatial point (or group of points) and the frequency domain information at any point (or group of points). Simulations were run on a Dell 690 workstation that is equipped with two 2.66 GHz 64-bit Dual-Core Intel® Xeon® 5150 series processors for a total of four execution cores in two sockets and 8 GB of RAM.
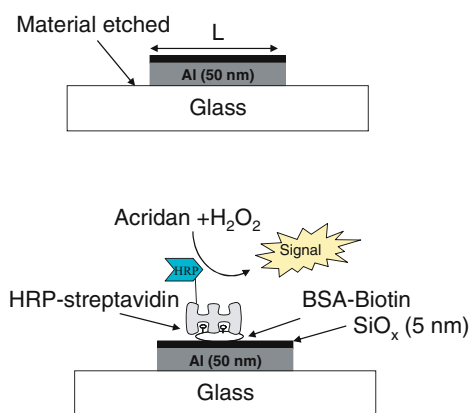
Fig. 1 Sample geometry scheme for aluminum square substrates (top) that are used for surface and solution assays (Fig. 3). Aluminum and SiOx layers are vapor deposited with thicknesses of 50 and 5 nm respectively. The material is then etched to form square Al/SiOx substrate geometries with a length (L). Scheme for BSA-biotin/HRP-streptavidin chemiluminescence surface assay is also shown (bottom)

Methods

Preparation of glass substrates modified with thin film aluminum triangles

Aluminum films approximately 50 nm thick were vapor deposited on silanized glass slides with an EMF Corp. (Ithaca, NY) instrument. Upon completion, a thin silicon monoxide layer 5 nm thick was vapor deposited to insure that surface protein interactions are approximately equivalent for glass and metal substrates. Square geometries, with lengths 2.5, 5, 10 and 20 mm, were etched into the thin film aluminum substrates for metal surface and solution chemiluminescence emission enhancement comparisons (Fig. 3). Slides modified with aluminum square substrates were cut into approximately 1 × 1.5 in^2 rectangles.

Preparation of the model protein assay (Biotin-Avidin) on aluminum films and glass substrates

The model assay used in this paper is based on the well-known interactions of biotin and avidin. Biotin groups are introduced to the glass and metal surfaces through biotinylated-BSA, which readily forms a monolayer on the surfaces of glass [36–38]. Surface luminescent decay experiments were carried out by incubating 5 μl of 10 nM biotinylated-BSA solutions in the Al and glass imaging chambers for approximately 1 hour. Chambers were washed with water to remove the unbound material. Imaging chambers were then incubated with 20 μl of 1% aqueous BSA (w/v) for one and a half hours to minimize non-specific binding of HRP-streptavidin to surfaces. Chambers were again washed with water to remove the BSA blocking solution. Stock solutions of HRP-streptavidin were diluted 1:25 to a final approximate

concentration of 10 μg/ml. Five microliters of the HRP-streptavidin solution was subsequently added into the imaging chambers affixed to the biotinylated-BSA coated glass and Al modified substrates and typically incubated at room temperature for approximately 30 minutes. Following incubation, imaging chambers were again washed with water to remove unbound HRP-streptavidin material and the chemiluminescence solution was subsequently added. In all of the experiments performed with low power microwaves, there was no evidence of surface drying. Solution assays (Fig. 3) were performed by mixing the chemiluminescence reagents as described in section 2.2.3, and 2 μl of 200 ng/ml of HRP-streptavidin solution, to the chemiluminescence reagents to *trigger* the reaction.

HRP-catalyzed chemiluminescence from reagents on Al and glass surfaces

The chemiluminescence experiments were performed with and without microwave (Mw) heating inside the microwave cavity (0.7 cu ft, GE Compact Microwave Model: JES735BF, max power 700 W). During microwave heating, 10 second pulses were applied at three or four 50 second intervals. The pulses were applied at 10%, 20%, 30% or 40% power respectively, which corresponded to 70, 140, 210, and 280 W over the entire cavity. Solutions A and B were mixed in different proportions to optimize chemiluminescence signal for these experiments. As a result, we measured the maximum emission signal from a 20:1 mixture of solution A to B. Subsequently, all reactions were performed by combining 40 μl of solution A with 2.0 μl of solution B and immediately adding the entire solution to the imaging chamber. Data collection commenced immediately following addition of reagents, and terminated when the photon counts returned to baseline. Histogram plots (Figs. 2 and 3) reflect maximum signal counts detected before an initial microwave pulse (no Mw) and after the application of microwave pulse trains (Mw).

Chemiluminescence reagents (Chemical reaction assay)

The commercially available glow-sticks contain the necessary reacting chemicals, which are enclosed within a plastic tube, and yield a bright chemiluminescent emission when they are physically altered. The plastic tube contains a phenyl oxalate ester and a fluorescent probe, where the choice of dye simply determines the color of the luminescence [39]. For the work undertaken here, this choice is arbitrary as long as the luminophore emits in the visible spectral region, consistent with previous reports [40]. Inside the plastic tube lies a glass capsule containing the activating agent (hydrogen peroxide). Activation of the chemicals is accomplished with a bend, snap, and a vigorous shake of the
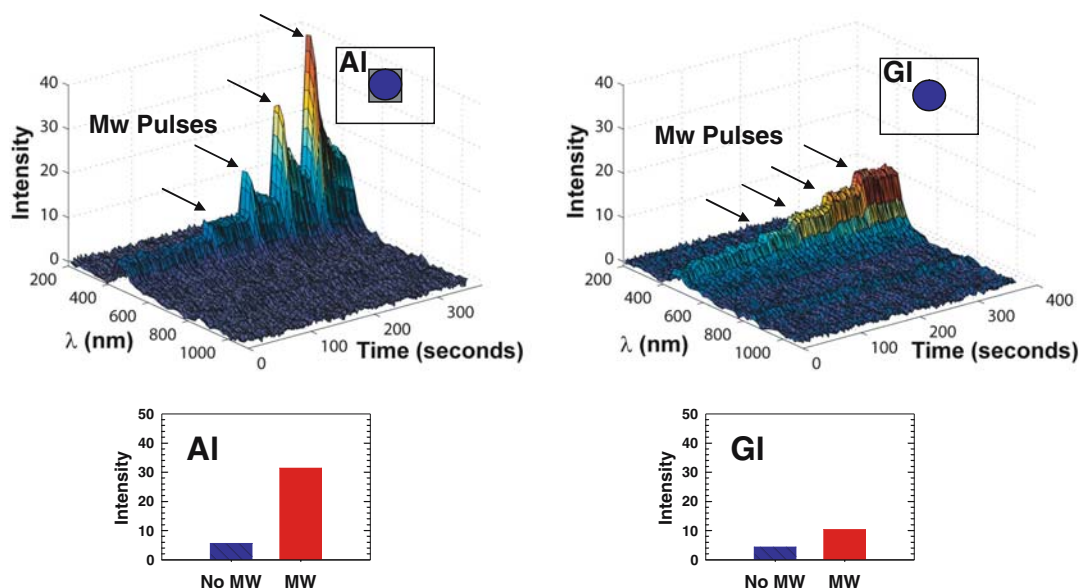
Fig. 2 3D time traces of chemiluminescence emission spectra from 40μl acridan/peroxide solution (insets, blue circles) on aluminum/SiOx (Al, top left; inset, grey box) and glass (Gl, top right; inset, white rectangle) substrates incubated with BSA-biotin/HRP-streptavidin complexes. Low power microwave pulses (Mw pulses) are applied at 50 second intervals for 10 seconds at 70 W, 140 W, 210 W and 280 W. Chemiluminescence emission intensity histograms before (blue bars) and after (red bars) exposure to microwave pulses from aluminum (bottom left) and glass substrates (bottom right) coated with BSA-biotin/HRP-streptavidin complexes. Aluminum films 50 nm thick and a subsequent SiOx 5 nm thick layer were vapor deposited onto glass substrates. Substrate surfaces were then incubated with 50 nM BSA-biotin and 10 mg/ml solution of HRP-streptavidin

plastic tube which breaks the glass capsule containing the peroxide and mixes the chemicals to begin the chemiluminescence reaction. The hydrogen peroxide oxidizes the phenyl oxalate ester to a peroxyacid ester and phenol. The unstable peroxyacid ester decomposes to a peroxy compound and phenol, the process chemically inducing an electronic excited state. Commercially available chemiluminescence materials were purchased and used to demonstrate the utility of the microwave-focused chemiluminescence approach.

Chemiluminescence images (Fig. 5) from square aluminum substrates with a length of 11 mm were acquired by affixing 2.5 mm imaging chambers at the 4 corners of the etched square geometry and one chamber at the center of the square. Subsequently, 6 μl of solution was placed in each of the imaging chambers and the images were recorded before and after the application of a 5 second, low power (70 W) microwave pulse.

Chemiluminescence detection

Chemiluminescence spectra were collected using an Ocean Optics spectrometer, model SD 2000 (Dunedin, FL), connected to an Ocean Optics 1000 μm diameter fiber with an NA of 0.22 (Dunedin, FL). The fiber was positioned vertically on top of the slides containing the chemiluminescent reagents inside the microwave cavity. Chemiluminescent spectra and time-dependent emission intensity were

collected with an integration time of 1 second for approximately 500 seconds unless otherwise noted. The integration time was kept constant between the control and aluminum film sample measurements.

The *real-color* photographs were taken with an Olympus Digital camera (C-740, 3.2 Mega Pixel, 10 × Optical Zoom) without the need for optical filters.

FDTD simulations and theory

Two-dimensional square structures were created with the FDTD simulation software. In order to model the 2-D equilateral aluminum square geometry that best approximated electric field intensity (E_x^2 and E_y^2) distributions for aluminum square geometry substrates, simulations were performed for sizes that approximated the large (10 mm × 10 mm) and small (2 mm × 2 mm) square geometries used in these experiments (Fig. 4). Optical properties of square structures were defined as perfect conductors. Thus, the total complex permittivity of a perfect conducting metal, such as aluminum, in the presence of a microwave field is given by;

$$\tilde{\varepsilon}(f) = \varepsilon_{\text{REAL}} + i\varepsilon_{\text{IMAG}} \frac{f_{\text{SIM}}}{f} + i\frac{\sigma}{2\pi \cdot f \varepsilon_o} \quad (1)$$

where ε_{REAL} is the real part of the permittivity for the dielectric medium, $\varepsilon_{\text{IMAG}}$ is the imaginary part of the
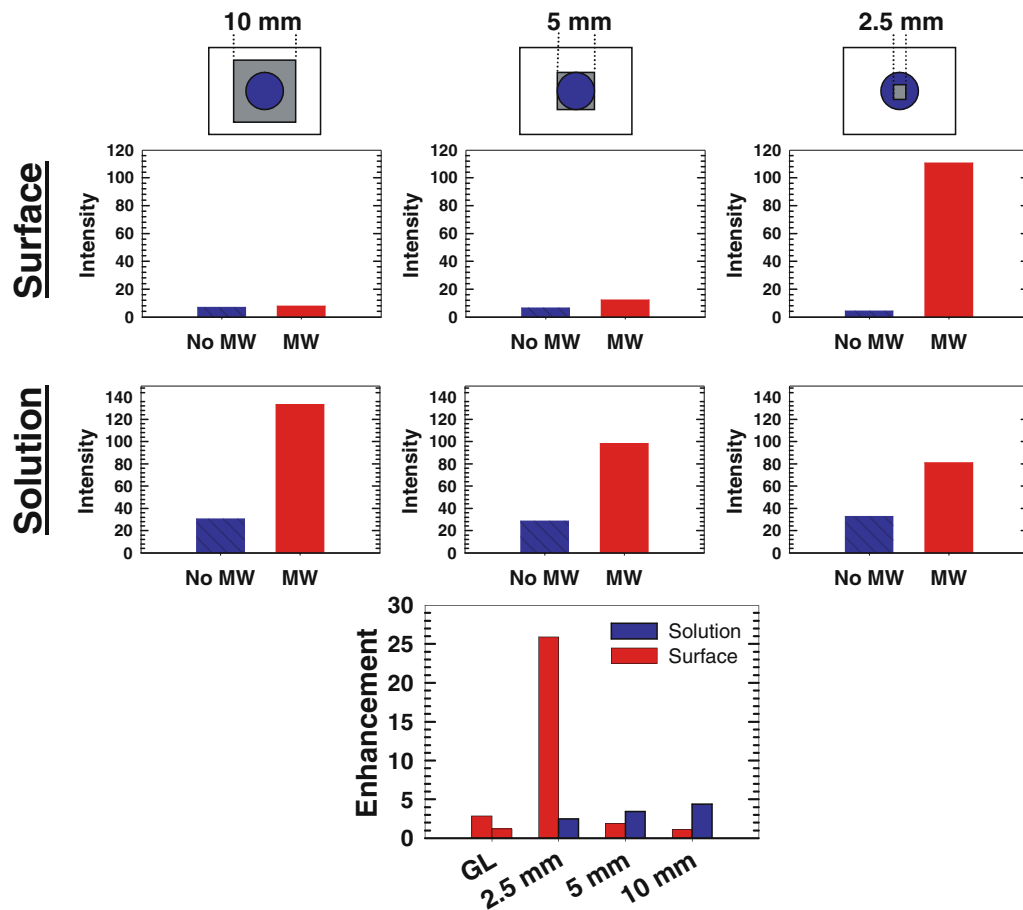
Fig. 3 Chemiluminescence intensity histograms before (blue bars) and after (red bars) exposure to microwave (Mw) pulses for surface bound HRP (top 3 panels) and HRP in solution (middle 3 panels) on continuous Al films 50 nm thick with 5 nm thick SiOx layers with square geometries of lengths 10, 5, and 2.5 mm (grey boxes). Surfaces were treated with 10 nM BSA-biotin and 20 μg/ml solution of HRP-streptavidin, and 40 μl of acridan/peroxide solution (blue circles) was subsequently added to an imaging chamber affixed to metal substrates. For solution assays, 2 μl of a 20 μg/ml HRP solution was added to 40 μl of acridan/peroxide. Maximum intensity after Mw (red bars) is divided by maximum intensity before initial Mw pulse (blue bars) to give enhancement ratios (bottom)

dielectric medium, f_{SIM} is the center frequency of all the sources in the simulation, f is the frequency of the simulation, ε_o is the permittivity of free space, and σ is the conductivity of the metal [41]. The conductivity value of the metal is approximated to be close to the d.c. value for aluminum [42], $3.8 \times 10^7 \text{Sm}^{-1}$, the background dielectric media is presumed to be air, and the frequency, f, is set to 2.45 GHz.

The microwave cavity source used in these experiments was a standard microwave oven that is equipped with a magnetron placed on the outside of the cavity, which is treated with white reflective coating to optimize microwave confinement, standing wave generation, and minimize absorption loss. We modeled this microwave system as a total field scattered electric field (TFSF) to best approximate the electromagnetic field in the microwave cavity during operation and assumed that only TE_{10} modes could propagate in the microwave cavity [43]. Subsequently, electromagnetic radiation is modeled to propagate from left to right along the x-axis across 2-D square structures. Mesh sizes were set at .1 mm and the simulation time is set to 10 ns to insure that the light travels down the surface and back. The absorbing boundary conditions are of the perfectly matched layer type and are used to truncate the FDTD domain in the *x* and *y* dimensions [41].

Results and discussion

In order to demonstrate the potential utility of aluminum substrates to further increase enhancements observed for the MT-MEC platform, we constructed a simple surface assay as described in the experimental section and shown in Fig. 1. Briefly, aluminum thin films 50 nm thick were vapor deposited onto silanated glass slides. In addtion, silicon monoxide layers 5 nm thick were also deposited onto the aluminum substrates, such that surface protein interactions to aluminum and glass are similar.
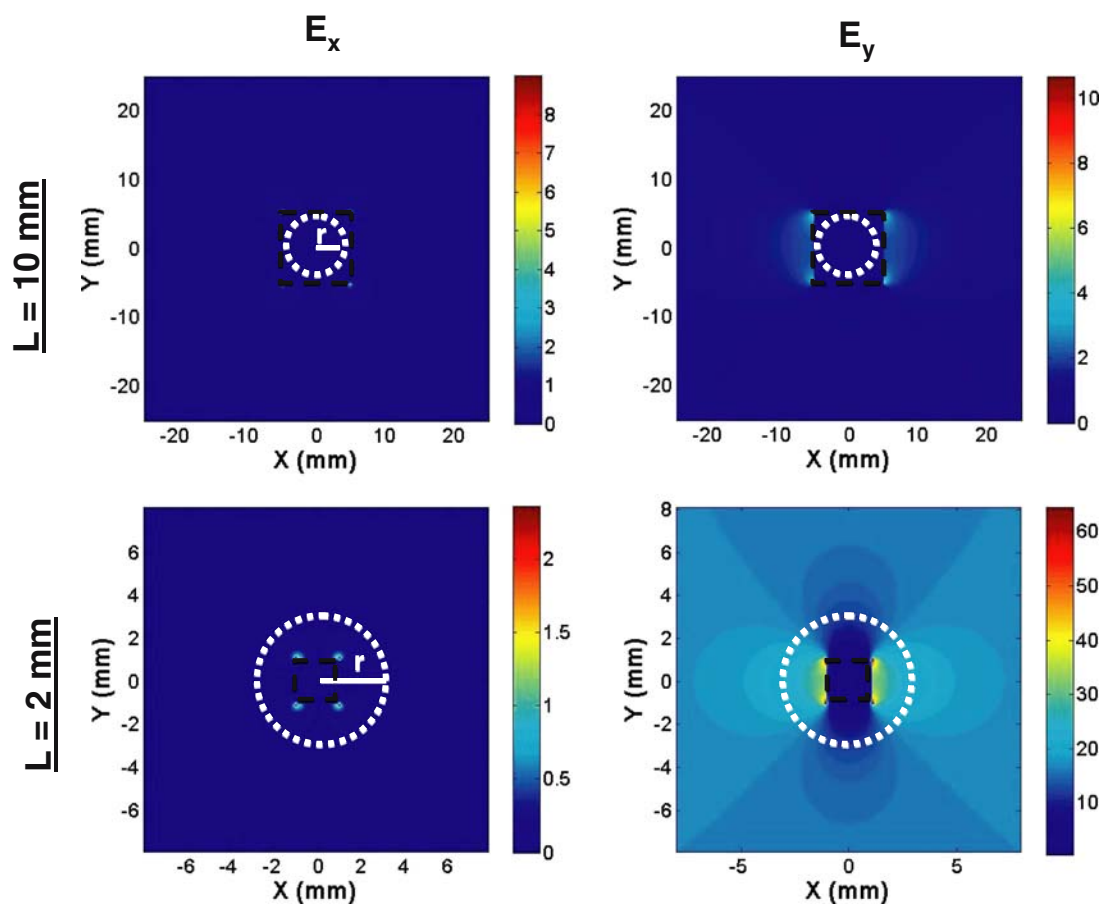
Fig. 4 Representative simulated intensity images, I_x (left) and I_y (right) of the electromagnetic field distribution for 2.45 GHz microwave frequencies incident upon aluminum squares with lengths of 10 mm (top panels) and 2 mm (bottom panels). The incident field is modeled as a total field scattered field (TFSF) with TE polarization and propagates from left to right. 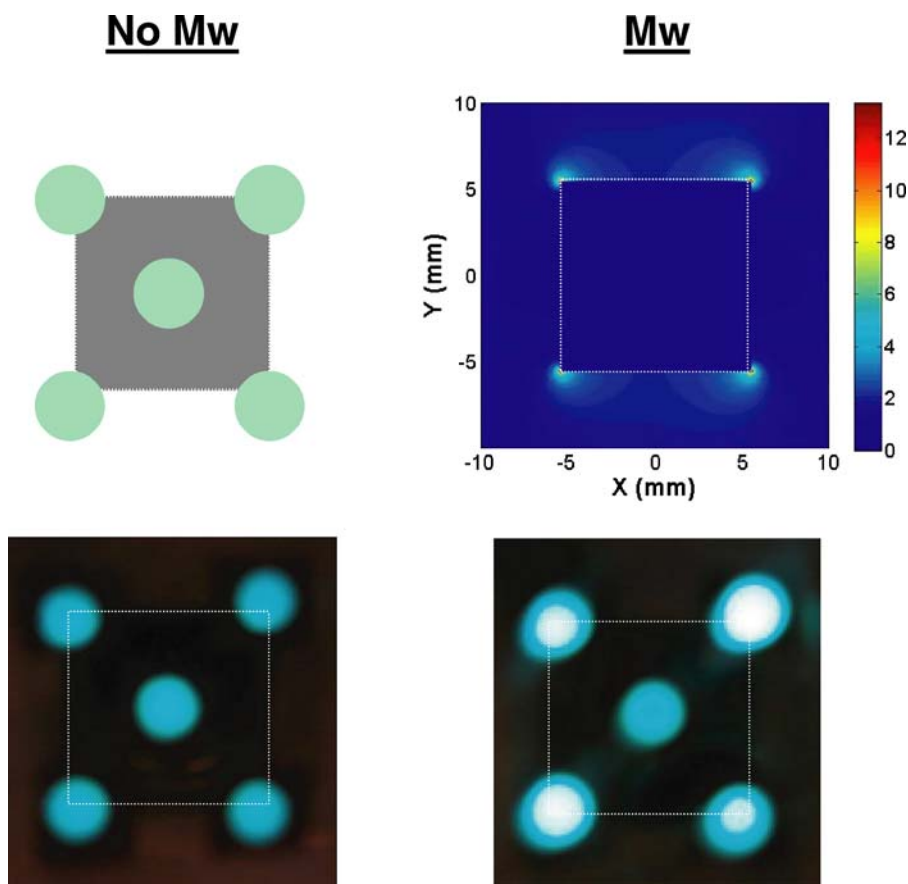Dashed black region approximates simulation region defined as planar aluminum square. Dotted white region approximates the relative coverage area ($r = 2.5$ mm) of the imaging chamber with chemiluminescence solution that yielded the experimental results in Figs. 2 and 3. Note: dotted regions are drawn to scale with respect to 10 mm and 2 mm simulation intensity images

To demonstrate the relative enhancements achieved with aluminum substrates, 10 nM biotinylated-BSA was incubated onto glass substrates and aluminum substrates etched to best approximate the area of an affixed imaging chamber, which is 5 mm diameter. HRP-streptavidin is then added to the surface, localizing the enzyme catalyst in close proximity to the aluminum substrate. The peroxide and acridan (lumophore) are then added to initiate the chemiluminescence reaction. Subsequently, we recorded spectral traces for the reaction on the aluminum (Fig. 2, top left) and glass substrates (Fig. 2, top right) at 1 second time intervals for 400 seconds. During the 400 second detection times, the aluminum (Al) and glass (Gl) substrates were exposed to four, 10 second low power microwave pulses (70 W, 140 W, 210 W, and 280 W respectively) at fifty second time intervals (arrows, Fig. 2, top). Prior to the application of equivalent microwave pulse trains to glass and aluminum protein treated substrates, we measure the maximum signal achieved from the steady chemilumi-

nescence emission that is reflective of the HRP catalyzed chemiluminescence reaction (blue bars, Fig. 2 bottom). Following the application of the low power Mw pulses, we measure the maximum signal achieved from the 'triggered' enzyme catalyzed chemiluminescence reaction (red bars, Fig. 2, bottom). In the presence of the aluminum substrate, the application of low power microwave pulses *dramatically increases the photon flux* from the chemiluminescence reaction (Fig. 2, left). As we have previously shown, this result is reflective of an accelerated reaction in the presence of a metal substrate [1, 2, 12].

During the course of our experiments, we observed that upon application of low power microwave pulses, 10×10 mm² aluminum substrates were slightly warmer than the glass substrates that were not treated with aluminum films. Thus, we questioned whether the relative enhancement that we observed for the aluminum substrate was a heating effect, and the relative enhancements from aluminum

Fig. 5 The sample geometry depicts the chemiluminescence sample (green circles) and aluminum/SiOx square substrate (top left; grey square, approximately 11 mm length). Without an incident low power microwave pulse, the chemiluminescence signal is approximately equivalent for all sample geometries (bottom left). Upon application of low power 2.45 GHz microwave pulses (for simulation results, E field is simulated as a TE polarized TFSF and propagates across the geometries from left to right), the experimental localized signal enhancement at the corners of the square aluminum substrate (bottom right) correlates with simulated total field intensity distributions ($I_x + I_y$, top right)

substrates are dependent on the size of the aluminum substrates, i.e. larger enhancements arose from larger aluminum surface area. Subsequently, we etched 20×20 mm² aluminum squares on glass substrates and prepared the surface assay as shown in Fig. 1. Upon application of the low power microwave pulses, we noted sparking or dielectric breakdown of the aluminum substrate. Consequently, we concluded that it may be more appropriate to decrease the size of the aluminum substrates and measure the resulting enhancements.

Aluminum square geometries with lengths 10 mm, 5 mm and 2.5 mm were prepared and functionalized with the BSA-biotin/HRP-streptavidin complexes and exposed to three 10 second microwave pulses (70 W, 140 W, and 210 W, respectively) at 50 second time intervals. In addition, solution assays were performed (see Methods and Materials section 2.2.2) and also exposed to the aforementioned microwave pulse trains. Solution experiments were performed to determine if the heating is localized to the surface (as reported for the previously published MT-MEC result for silver island films [1, 2, 12]), strictly due to solution heating, or a combination of both phenomena. Prior to the application of equivalent microwave pulse trains to glass and aluminum protein treated substrates, we again measured the maximum signal achieved

from the steady chemiluminescence emission that is reflective of the HRP catalyzed chemiluminescence reaction (blue bars, Fig. 3). Following the application of pulses, we measure the maximum signal achieved from the 'triggered' enzyme catalyzed chemiluminescence reaction (red bars, Fig. 3). In the presence of the 2.5×2.5 mm² square aluminum substrates, maximum photon flux is achieved from the surface chemiluminescence reactions (Fig. 3, top right), while minimum enhancements are noted for the 5×5 mm² (Fig. 3, top center) and 10×10 mm² square aluminum substrates (Fig. 3, top left). On the other hand, solution studies show an opposing trend (Fig. 3, middle panels). In the presence of the 10×10 mm² square aluminum substrates, maximum 'triggered' photon flux is achieved from the solution based chemiluminescence reactions (Fig. 3, middle left), while minimum enhancements are noted for the 5×5 mm² (Fig. 3, middle center) and 2.5×2.5 mm² (Fig. 3, middle right) square aluminum substrates. The maximum enhancements for surface (> 25-fold, red bars) and solution (> 4-fold, blue bars) reactions demonstrate marked increases in photon flux for microwave triggered enzyme catalyzed chemiluminescent reactions from aluminum substrates (Fig. 3, bottom middle). Enhancements are representative of maximum chemiluminescence emission after the applications of the Mw pulse

train divided by the maximum emission before the initial application of a Mw pulse.[1]

Our FDTD calculations show that the four corners of the square geometries exhibit the maximum electric field enhancements (Fig. 4). Because similar radiation maxima locations were observed for 2 D and 3 D simulations (data not shown), we used 2 D FDTD simulations to demonstrate the relative electric field distributions [44]. Square planar structures are assumed to be an infinite column and act as an electromagnetic condenser. Thus, these structures are acting as lightening rods for charge buildup at the corners of the squares to drive the chemical reactions. Since the fields for the square geometries are localized at the corners, it is evident that the field enhancements for the larger square geometries (Fig. 4, top) will lie outside the region of the imaging chamber, which is approximately 5 mm in diameter (Fig. 4, dotted circles). On the other hand, the smaller square geometries will have field enhancements within the region of the imaging chamber (Fig. 4, bottom). Since the field enhancements for the smaller geometries exist within the sample region (white dotted circle) and enhancements spread into surrounding areas (E_y^2 intensities, Fig. 4, bottom left), we believe that these fields are the source of the significant surface enhancements noted for the 2.5×2.5 mm^2 square geometries. In contrast, for the larger geometries, the fields lie well outside the sample region (Fig. 4 bottom, dashed circle) and the solution signal enhancements are simply explained by ohmic heating of the aluminum and glass substrates.

Finally, we etched a square aluminum/SiOx substrate with a length of 11 mm on a glass slide as previously described. Subsequently we affixed 2.5 mm chamber wells at the four corners of the square geometry and one chamber well at the center of the square and filled them with 6 μl of green chemiluminescence solution (Fig. 5, top left). Prior to applying low power microwave pulse, we recorded an image of the luminescent material. The intensity of the material at the five positions on the squares was approximately equivalent (Fig. 5, bottom left). Upon application of a five second, low power microwave pulse (70 W), we observed dramatic signal enhancements from the chemiluminescence solution at the four corners of the square Al/SiOx substrate (Fig. 5, bottom right),

and a *slight* intensity increase for the solution at the center of the square. When these results are directly compared with FDTD simulation total intensity ($I_x + I_y$) images (Fig. 5, top right), we note that the simulation results are reproduced experimentally. We also note that that the slight intensity increase for the solution at the center of the square geometry may result again from ohmic heating or microwave heating from the standing waves in the microwave cavity that are unaffected by the aluminum geometries. Only further surface and solution temperature studies will provide further insight into the nature of these results, but these preliminary results suggest that maximum signal enhancement for surface and solution reactions can be achieved by optimizing aluminum substrate geometries.

Conclusions

Combining the advantages of MT-MEC with optimized aluminum planar geometries, we believe that we can further improve the sensitivity and rapidity of surface and solution protein detection with chemiluminescence. Using optimized aluminum geometrical planar structures to localize microwave field enhancements, we have shown that we can focus microwave fields and control the extent and location of field enhancements, such that we can not only *temporally* 'trigger' chemiluminescent reactions, but also *spatially* 'trigger' these reactions. We observed > 25-fold and > 4-fold enhancements for surface and solution reactions respectively. With these dramatic 'on demand' increases in photon flux from 'triggered' chemiluminescent reactions, we feel that we can provide an invaluable technology to present day work in microarray detection. We anticipate that the signal to noise and accelerated reaction rates generated from this new technology platform, Microwave Triggered Metal-Enhanced Chemiluminescence (MT-MEC) on aluminum planar geometrical substrates, can also be implemented to improve sensitivity, rapidity, specificity, and quantification of macromolecules, organic syntheses, cancer detection, cancer treatments, cellular studies and a host of other sensing technologies.

---

[1] With regard to the surface assays, the incubation chamber for the 2.5×2.5 mm^2 aluminum square sample has a small area of exposed glass. Consequently, we suspected that it is possible that protein adsorption to glass and Al coated with SiOx are not equivalent. The results in Fig. 3 would suggest that protein binds more readily to the glass than the aluminum, which would explain the dramatic surface enhancement for the smaller area aluminum substrates. If this was the case, the surface reaction results in Fig. 2 would display a similar trend, whereby the glass substrate would show greater enhancements than aluminum. Since this is not our observation, we believe that this effect is not an artifact of nonequivalent surface loading of the two substrates.

References

1. Previte MJR, Aslan K, Malyn S, Geddes CD (2006) Microwave-triggered metal-enhanced chemiluminescence (MT-MEC): Application to ultra-fast and ultra-sensitive clinical assays. J Fluorescence 16(5):641–647

2. Previte MJR, Aslan K, Malyn S, Geddes CD (2006) Microwave triggered metal-enhanced chemiluminescence: Quantitative protein determination. Anal Chem

3. Kricka LJ (ed) (2000) Bioluminescence and chemiluminescence, Pt C. pp 333–345

4. Burnette WN (1981) "Western blotting": Electrophoretic transfer of proteins from sodium dodecyl sulfate-polyacrylamide gels to unmodified nitrocellulose and radiographic detection with antibody and radioiodinated protein A Anal Biochem 112(2):195–203

5. Whitehead TP, Thorpe GHG, Carter TJN, Groucutt C, Kricka LJ (1983) Enhanced luminescence procedure for sensitive determination of peroxidase-labeled conjugates in immunoassay. Nature 306(5930):158–159.

6. Dubois R (1885) Note sur la physiologie des pyrophores. C R Soc Biol 2:559

7. Harvey EN (1957) A history of luminescence from the earlies times until 1900. The American Philosophical Society, Philiadelphia, PA

8. Kricka LJ (1994) In: Campbell AK, Kricka LJ, Stanley PE (eds) Bioluminescence and chemiluminescence: Fundamental and applied aspects. Wiley, Chichester

9. Ozinkas A (1994) In: Lakowicz JR (ed) Topics in fluorescence spectroscopy. Plenum Press, New York

10. Bange A, Halsall HB, Heineman WR (2005) Microfluidic immunosensor systems Biosens. Bioelectron 20(12):2488–2503

11. Chowdhury MH, Aslan K, Malyn SN, Lakowicz JR, Geddes CD (2006) Metal-enhanced chemiluminescence. J Fluorescence 16(3):295–299

12. Aslan K, Malyn SN, Geddes CD (2006). Multicolor microwave-triggered metal-enhanced chemiluminescence. J Am Chem Soc 128(41):13372–13373

13. Aslan K, Geddes CD (2005) Microwave-accelerated metal-enhanced fluorescence: Platform technology for ultrafast and ultrabright assays. Anal Chem 77(24):8057–8067

14. Whittaker AG, Mingos DMP (1995) Microwave-assisted solid-state reactions involving metal powders. J Chem Soc Dalton Trans 12:2073–2079

15. Sridar V (1998) Microwave radiation as a catalyst for chemical reactions. Curr Sci 74(5):446–450

16. Sridar V (1997) Rate acceleration of Fischer-indole cyclization by microwave irradiation. Indian J Chem Sect B-Org Chem Incl Med Chem 36(1):86–87

17. Varma RS (2002) Advances in green chemistry: Chemical synthesis using microwave irradiation. Astrazeneca Research Foundation, Banglore, India

18. Caddick S (1995) Microwave assisted organic reactions. Tetrahedron 51:10403–10432

19. Lin JC, Yuan PMK, Jung DT (1998) Enhancement of anticancer drug delivery to the brain by microwave induced hyperthermia. Bioelectrochem Bioenerg 47(2):259–264

20. Akins RE, Tuan RS (1995) Ultrafast protein determinations using microwave enhancement. Mol Biotechnol 4(1):17–24

21. Croppo GP, Visvesvara GS, Leitch GJ, Wallace S, Schwartz DA (1998) Identification of the microsporidian Encephalitozoon hellem using immunoglobulin G monoclonal antibodies. Arch Pathol Lab Med 122(2):182–186

22. Philippova TM, Novoselov VI, Alekseev SI (1994) Influence of microwaves on different types of receptors and the role of peroxidation of lipids on receptor-protein shedding. Bioelectromagnetics 15(3):183–192

23. VanTriest B, Loftus BM, Pinedo HM, Backus HHJ, Schoenmakers P, Telleman F, Tadema T, Aherne GW, Van Groeningen CJ, Zoetmulder FAN, Taal BG, Johnston PG, Peters GJ (2000) Thymidylate synthase expression in patients with colorectal carcinoma using a polyclonal thymidylate synthase antibody in comparison to the TS 106 monoclonal antibody. J Histochem Cytochem 48(6):755–760

24. Rhodes A, Jasani B, Balaton AJ, Barnes DM, Anderson E, Bobrow LG, Miller KD (2001) Study of interlaboratory reliability and reproducibility of estrogen and progesterone receptor assays in Europe—Documentation of poor reliability and identification of insufficient microwave antigen retrieval time as a major contributory element of unreliable assays. Am J Clin Pathol 115(1):44–58

25. Bismuto E, Mancinelli F, d'Ambrosio G, Massa R (2003) Are the conformational dynamics and the ligand binding properties of myoglobin affected by exposure to microwave radiation? Eur Biophys J Biophys Lett 32(7):628–634

26. Roy I, Gupta MN (2003) Applications of microwaves in biological sciences. Curr Sci 85(12):1685–1693

27. Porcelli M, Cacciapuoti G, Fusco S, Massa R, dAmbrosio G, Bertoldo C, DeRosa M, Zappia V (1997) Non-thermal effects of microwaves on proteins: Thermophilic enzymes as model system. FEBS Lett 402(2–3):102–106

28. Chen LF, Ong CK, Neo CP, Varadan VV, Varadan VK (2004) Microwave electronics measurement and materials characterization. John Wiley & Sons Ltd., Chichester

29. Liao PF, Wokaun A (1982) Lightning rod effect in surface enhanced raman-scattering. J Chem Phys 76(1):751–752

30. Kappe CO (2002) High-speed combinatorial synthesis utilizing microwave irradiation. Curr Opin Chem Biol 6(3):314–320

31. Schweitzer B, Kingsmore SF (2002) Measuring proteins on microarrays. Curr Opin Biotechnol 13(1):14–19

32. Lin JC (1986) Special issue on phased-arrays for hyperthermia treatment of cancer—foreword. IEEE Trans Microw Theory Tech 34(5):481–483

33. Arber SL, Lin JC (1984) Microwave enhancement of membrane conductance - Effects of Edta, Caffeine and Tetracaine. Physiol Chem Phys Med NMR 16(6):469–475

34. Arber SL, Lin JC (1985). Microwave-induced changes in nerve-cells - effects of modulation and temperature. Bioelectromagnetics 6(3):257–270

35. Jain S, Sharma S, Gupta MN (2002) A microassay for protein determination using microwaves. Anal Biochem 311(1):84–86

36. Green NM (1975) Adv Protein Chem 29:85–133

37. Wilchek M, Bayer EA (1988) The avidin-biotin complex in bioanalytical applications. Anal Biochem 171(1):1–32

38. Wilchek M, Bayer EA (1990) Applications of avidin-biotin technology: literature survey. Method Enzymol 184:14–45

39. Lakowicz JR (1999) Principles of fluorescence spectroscopy, 2nd edn. Kluwer Academic, New York

40. Aslan K, Lakowicz JR, Geddes CD (2005) Plasmon light scattering in biology and medicine: New sensing approaches, visions and perspectives. Curr Opin Chem Biol 9(5):538–544

41. I Lumerical Solutions (2006) FDTD solutions manual release 4.0. Vancouver, BC

42. Suckling JR, Hibbins AP, Lockyear MJ, Preist TW, Sambles JR, Lawrence CR (2004) Finite conductance governs the resonance transmission of thin metal slits at microwave frequencies. Phys Rev Lett 92(14)

43. Hanafusa S, Iwasaki T, Nishimura N (1994) "Electromagnetic field analysis of a microwave oven by the FD-TD method-a consideration on steady state analysis," presented at Antennas and Propagation Society International Symposium, 1994. AP-S. Digest

44. Radzevicius SJ, Chen CC, Peters L, Daniels JJ (2003) Near-field dipole radiation dynamics through FDTD modeling. J Appl Geophys 52(2–3):75–91